Seismic Signatures of Fractured Rocks: Numerical Considerations using the Rotated Staggered Finite Difference Grid

E. H. Saenger, O. S. Krüger, and S. A. Shapiro

email: *saenger@geophysik.fu-berlin.de*

keywords: *rotated staggered FD grid, viscoelastic wave propagation, diffraction, fractures, effective rock properties*

ABSTRACT

This paper is concerned with numerical tests of rock physical relationships. The focus is on effective velocities in fractured media. We apply the so-called rotated staggered finite difference grid (RSG) technique. Using this modified grid it is possible to simulate the propagation of elastic waves in a 2D or 3D medium containing cracks, pores or free surfaces without hard-coded boundary conditions. It is shown that the RSG can be applied in displacement-stress and in velocity-stress finite-difference schemes whereby the latter is advantageous to model viscoelastic wave propagation. A comparison of the analytical solution for the wavefield at a single crack with the numerical result using the RSG shows an excellent agreement. Therefore the RSG allows an efficient and precise numerical study of effective velocities in fractured structures. We model the propagation of plane waves through a set of randomly cracked 3D media. In these numerical experiments we vary the crack density. The synthetic results are compared with several theories that predict the effective P- wave velocities in such materials. For randomly distributed and randomly oriented penny-shaped dry cracks the numerical simulations of P-wave velocities are in good agreement with the predictions of the self-consistent approximation.

INTRODUCTION

The problem of effective elastic properties of fractured solids is of considerable interest for geophysics, material science, and solid mechanics. Strong scattering caused by many dry cracks can be treated only by numerical techniques because an analytical solution of the wave equation is not available. In this paper we consider the problem of a fractured medium in two and three dimensions.

Finite difference (FD) methods discretize the wave equation on a grid. They replace spatial derivatives by FD operators using neighboring points. The wave field is also discretized in time, and the wave field for the next time step is generally calculated by using a Taylor expansion. Elastic FD methods can be separated in displacement-stress FD methods (Dablain, 1986), using the 2nd order wave equation, and velocity stress methods, solving two coupled first order equations (Virieux, 1986). Since the FD approach is based on the wave equation without physical approximations, the method accounts not only for direct waves, primary reflected waves, and multiply reflected waves, but also for surface waves, head waves, converted reflected waves, and waves observed in ray-theoretical shadow zones (Kelly et al., 1976).

Velocity stress FD schemes are normally used for viscoelastic wave propagation. This fact results in the basic numerical procedure which is described in section "The velocity-stress FD scheme". The RSG can also be implemented in this FD scheme to simulate the propagation of viscoelastic waves in a 2D or 3D medium containing cracks, pores or free surfaces without hard-coded boundary conditions.

A keypoint in numerical modeling is accuracy. There are only a limited number of analytical solutions of wave propagation in fractured media available. In section "The diffraction of SH waves by a finite crack" we compare an analytical solution given by Sánchez-Sesma and Iturrarán-Viveros (2001) with the numerical solution using the RSG.

We conclude this paper with a numerical study of effective velocities of fractured 3D-media (numerical results of 2D-media with intersecting and non-intersecting rectilinear thin dry cracks can be found in Saenger and Shapiro (2001)). Here we model the propagation of plane waves through a well defined fractured region with dry penny-shaped cracks. Theories of effective velocities, the numerical setup and our results are described and discussed in section "Effective velocities in 3D fractured media".

THE VELOCITY-STRESS FD SCHEME

3D viscoelastic wave equations

In this section we describe the velocity-stress formulation of the system of differential equations which were the basis for the FD implementation. As shown below viscoelasticity can be implemented in a very efficient way. A derivation of these equations can be found for example in Robertsson et al. (1994).

The stress-strain relation for a generalized standard linear solid reads:

$$\begin{aligned}\dot{\sigma}_{ij} &= \frac{\partial v_k}{\partial x_k}\left\{\pi\left[1+\sum_{l=1}^{L}\left(\frac{\tau_{\epsilon l}^{p}}{\tau_{\sigma l}}-1\right)\right]-2\mu\left[1+\sum_{l=1}^{L}\left(\frac{\tau_{\epsilon l}^{s}}{\tau_{\sigma l}}-1\right)\right]\right\}\\ &\quad +2\frac{\partial v_i}{\partial x_j}\mu\left[1+\sum_{l=1}^{L}\left(\frac{\tau_{\epsilon l}^{s}}{\tau_{\sigma l}}-1\right)\right]+\sum_{l=1}^{L} r_{ijl} \qquad \text{if} \quad i=j, \qquad (1)\\ \dot{\sigma}_{ij} &= \left(\frac{\partial v_i}{\partial x_j}+\frac{\partial v_j}{\partial x_i}\right)\mu\left[1+\sum_{l=1}^{L}\left(\frac{\tau_{\epsilon l}^{s}}{\tau_{\sigma l}}-1\right)\right]+\sum_{l=1}^{L} r_{ijl} \qquad \text{if} \quad i\neq j \qquad (2)\end{aligned}$$

with the so-called memory equations:

$$\dot{r}_{ijl} = -\frac{1}{\tau_{\sigma l}}\left\{\frac{\partial v_k}{\partial x_k}\left[\pi\left(\frac{\tau^p_{\epsilon l}}{\tau_{\sigma l}}-1\right)-2\mu\left(\frac{\tau^s_{\epsilon l}}{\tau_{\sigma l}}-1\right)\right] 2\frac{\partial v_i}{\partial x_j}\mu\left(\frac{\tau^s_{\epsilon l}}{\tau_{\sigma l}}-1\right)+r_{ijl}\right\} \quad \text{if} \quad i=j, \tag{3}$$

$$\dot{r}_{ijl} = -\frac{1}{\tau_{\sigma l}}\left\{\mu\left(\frac{\tau^s_{\epsilon l}}{\tau_{\sigma l}}-1\right)\left(\frac{\partial v_i}{\partial x_j}+\frac{\partial v_j}{\partial x_i}\right)+r_{ijl}\right\} \quad \text{if} \quad i\neq j \tag{4}$$

The equation of momentum conservation:

$$\rho_g\frac{\partial v_i}{\partial t} = \frac{\sigma_{ij}}{\partial x_j}+f_i \tag{5}$$

completes the system of first order coupled partial differential equations which describe seismic wave propagation in a 3-D viscoelastic medium. Following Bohlen (1998) we use the variables $\tau^p=(\tau^p_{\epsilon l}/\tau_{\sigma l}-1)$ and $\tau^s=(\tau^s_{\epsilon l}/\tau_{\sigma l}-1)$ in the numerical implementation. The dot over symbols indicates partial differentiation with respect to time. The meaning of the symbols is as follows:

$$\pi = v_p^2\rho_g\Re^2\left(\sqrt{\frac{1}{1+\sum_{l=1}^{L}\frac{i\omega_0\tau_{\sigma l}}{1+i\omega_0\tau_{\sigma l}}\tau^p}}\right), \tag{6}$$

$$\pi = v_s^2\rho_g\Re^2\left(\sqrt{\frac{1}{1+\sum_{l=1}^{L}\frac{i\omega_0\tau_{\sigma l}}{1+i\omega_0\tau_{\sigma l}}\tau^s}}\right), \tag{7}$$

ω_0	center frequency of the source,
v_p	P wave phase velocity (at center frequency),
v_s	S wave phase velocity (at center frequency),
σ_{ij}	denotes the ijth component of the stress tensor,
v_i	denote the components of the particle velocities
x_i	indicate the three spatial directions (x,y,z)
r_{ijl}	are the L memory variables (l=1,...,L),
f_i	denotes the components of external body force
$\tau_{\sigma l}$	are the L stress relaxation times for both P- and S-waves
τ^p, τ^s	define the level of attenuation for P- and S-waves, respectively
ρ_g	is the gravitational density

The parameters $\tau_{\sigma l}$, τ^p and τ^s can be optimized for the desired Q-spectra (Bohlen, 1998).

Discretization

The coupled system of continuous differential equations presented above were recast into discretized equivalents using staggered-grid approaches. For the sake of simplicity, we consider

here isotropic elastic medium in two dimensions with equal grid spacing in **z**- and **x**-direction. However, the results shown in Fig. 1 are also transferable to rectangular cells in three dimensions and all kinds of anisotropic elastic media. For the viscoelastic case in Fig. 1(b) the parameters $\tau_{\sigma l}$, τ^p and τ^s have the same position as σ_{ij}.

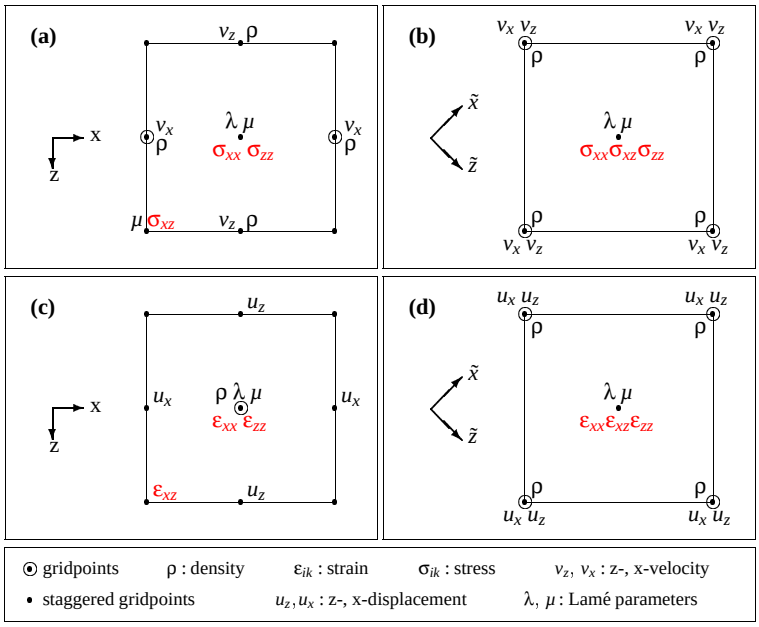

Figure 1: Elementary cells of different staggered grids. Locations where strains, displacements, velocities and elastic parameters are defined. **(a)** velocity-stress FD technique using a standard staggered grid. **(b)** velocity-stress FD technique using the rotated staggered grid. **(c)** displacement-stress FD technique using a standard staggered grid. **(d)** displacement-stress FD technique using the rotated staggered grid. Please note that for the RSG all components of one physical property are placed only at one location (**(b)** and **(d)**)

Numerical stability and dispersion

In Saenger et al. (2000) numerical stability and grid dispersion of the RSG is investigated. Though only the displacement-stress scheme is explicitly treated in this paper, all results also apply to the velocity-stress scheme (compare with Moczo et al. (2000)).

Therefore the stability criterion for velocity-stress RSG schemes (2nd order time) can be found in Saenger et al. (2000):

$$\frac{\Delta t v_p}{\Delta h} \leq 1/(\sum_{k=1}^{n} |c_k|). \tag{8}$$

In this equation c_k denotes the difference coefficients (e.g. Central Limit coefficients (Karrenbach, 1995)), v_p the compressional wave velocity, Δt the time increment, and Δh the grid spacing.

For 2nd order schemes in time and space we obtain the following dispersion relation for rotated staggered grid schemes (Saenger et al. (2000)):

$$\begin{aligned}\sin^2\left(\frac{\hat{\omega}\Delta t}{2}\right) &= \frac{\Delta t^2 v_{p,s}^2}{\Delta z^2}\sin^2\left(\frac{k_z\Delta z}{2}\right)\cos^2\left(\frac{k_x\Delta x}{2}\right)\cos^2\left(\frac{k_y\Delta y}{2}\right)\\ &+ \frac{\Delta t^2 v_{p,s}^2}{\Delta x^2}\cos^2\left(\frac{k_z\Delta z}{2}\right)\sin^2\left(\frac{k_x\Delta x}{2}\right)\cos^2\left(\frac{k_y\Delta y}{2}\right)\\ &+ \frac{\Delta t^2 v_{p,s}^2}{\Delta y^2}\cos^2\left(\frac{k_z\Delta z}{2}\right)\cos^2\left(\frac{k_x\Delta x}{2}\right)\sin^2\left(\frac{k_y\Delta y}{2}\right).\end{aligned} \tag{9}$$

This equation is the initial point of an extensive dispersion analysis which can be found in Saenger et al. (2000).

Modeling example

In this example we created a relatively simple 2D model. We want to demonstrate that the rotated grid can be applied for viscoelastic velocity-stress FD modeling (see Fig. 3) and can handle the high contrasts at four ('free') surfaces in the model. The model (gridspacing $\Delta h = 5m$) consists of a $2500m \times 2500m$ area in which the compressional and shear wave phase velocity is set to $v_p = 6300\ m/s$ and $v_s = 3637\ m/s$; the density is $\rho_g = 2100\ kg/m^3$. At the four boundaries around this area we set the velocities v_p and v_s to zero and the density to $\rho_g = 0.0001\ kg/m^3$. An explosion source ($f_{fund} = 33\ Hz,\ \Delta t = 0.0002s$) is placed at the point (520m,1520m). The modeling is done using 2nd order time update and 2nd order spatial differentiation operators. The corresponding Q-spectra using the viscoelastic parameters $\tau = \tau^p = \tau^s = 0.0353\ s$, $f_1 = 2\pi/\tau_{\sigma 1} = 8.2688\ 1/s$ and $f_2 = 2\pi/\tau_{\sigma 2} = 84.6761\ 1/s$ (L=2) is shown in Fig. 2.

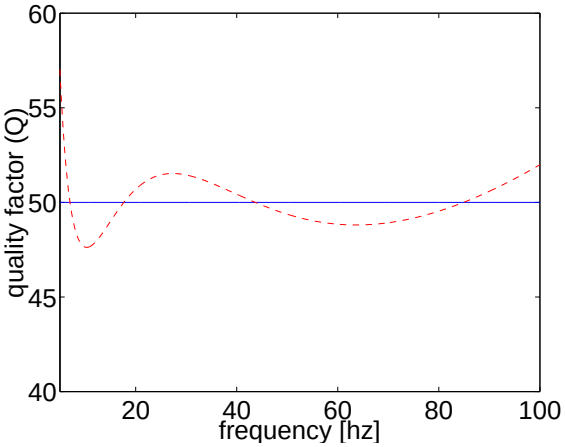

Figure 2: Desired Q-spectra for the modeling example.

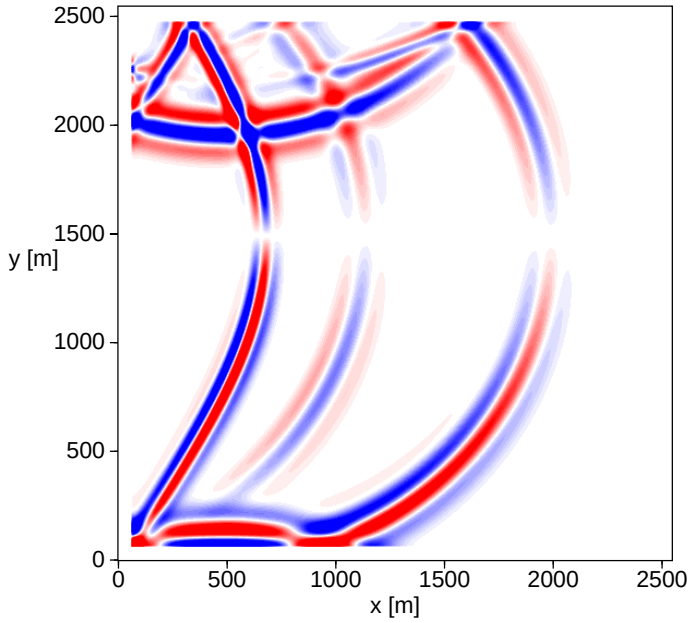

Figure 3: Modeling result using the viscoelastic velocity-stress rotated staggered FD grid. A snapshot (y-velocities) at $t = 0.28\ s$ is displayed.

THE DIFFRACTION OF SH WAVES BY A FINITE CRACK

Introduction

Checking the accuracy of the rotated staggered grid FD code described in (Saenger et al., 2000) we used an analytical solution for scattering and diffraction of SH waves by a finite crack given by Sánchez-Sesma and Iturrarán-Viveros (2001). They present a set of equations that allow the calculation of the frequency intensity distribution along the illuminated (Eq. 10) and shaded (Eq. 11) side of a finite crack with appropriate accuracy:

$$v^{(d)^-} = v_0^{(d)^-} + \frac{v_1 Z - v_2}{1 - Z^2} s(r_1) F(\sqrt{2kr_1}) + \frac{v_2 Z - v_1}{1 - Z^2} s(r_2) F(\sqrt{2kr_2}), \tag{10}$$

$$v^{(t)^+} = 2v_o e^{ikx \sin\gamma} - v^{(d)^-}, \tag{11}$$

where:

$$v_0^{(d)^-} = v_0[e^{-ika\sin\gamma} s(r_1) F\left(\sqrt{2kr_1}\sin\frac{\Theta_1}{2}\right) + e^{ika\sin\gamma} s(r_2) F\left(\sqrt{2kr_2}\sin\frac{\Theta_1}{2}\right)], \tag{12}$$

$$v_1 = v_0 e^{-ika\sin\gamma} s(2a) F\left(\sqrt{4ka}\sin\frac{\Theta_1}{2}\right), \tag{13}$$

$$v_2 = v_0 e^{ika\sin\gamma} s(2a) F\left(\sqrt{4ka}\sin\frac{\Theta_2}{2}\right), \tag{14}$$

and:

$$Z = s(2a)F(\sqrt{4ka}), \quad (15)$$

$$s(r) = (2/\sqrt{\pi})e^{ikr-\pi/4}, \quad (16)$$

$$F(z) = \exp(-iz^2)\int_z^\infty \exp(-i\tau)d\tau, \quad (17)$$

$$\Theta_1 = \pi/2 - \gamma, \quad (18)$$

$$\Theta_2 = \pi/2 + \gamma, \quad (19)$$

v_0 initial intensity,

k wavenumber,

$r_{1,2}$ position seen from the left or right end of the crack,

a half crack length,

γ incident angle of the wave field.

Our goal was to numerical implement a scenario of a plane SH wave interacting with a finite crack at an angle of 0^o (see Fig. 4) and to compare the numerical and analytical results. The model parameters were chosen as follows:

model	
dimensions	6200 $\times$ 5701 gridpoints (62cm x 57cm)
spacing	0.0001m in both directions
v_s	$2944\ m/s$
ρ_g	$2500\ kg/m^3$
wave	
type	ricker1 (first derivative of a Gaussian)
f_{dom}	100 kHz
crack	
length 2a	801 gridpoints (8cm)
v_s	$0\ m/s$
ρ	$0.000001\ kg/m^3$

Procedure

We chose one of several possible ways to compare the analytical and numerical results. We intended to convert the numerical values to normalized values as they are used in the analytical solution. Therefore the seismograms spectra had to be calculated. The source signal had to be segregated from the seismograms. This was done by dividing the seismogram spectra by the source signal spectrum. Finally two projections were made. The place of a geophone was projected on to the interval [-1 ; 1] (normalized crack; see Eq. 20) and the frequencies of the seismograms spectra had to be associated to the normalized frequencies (see Eq. 21).

$$\tilde{x} = (x-a)/a, \quad (20)$$

$$\tilde{f} = 2fa/v_s \quad (21)$$

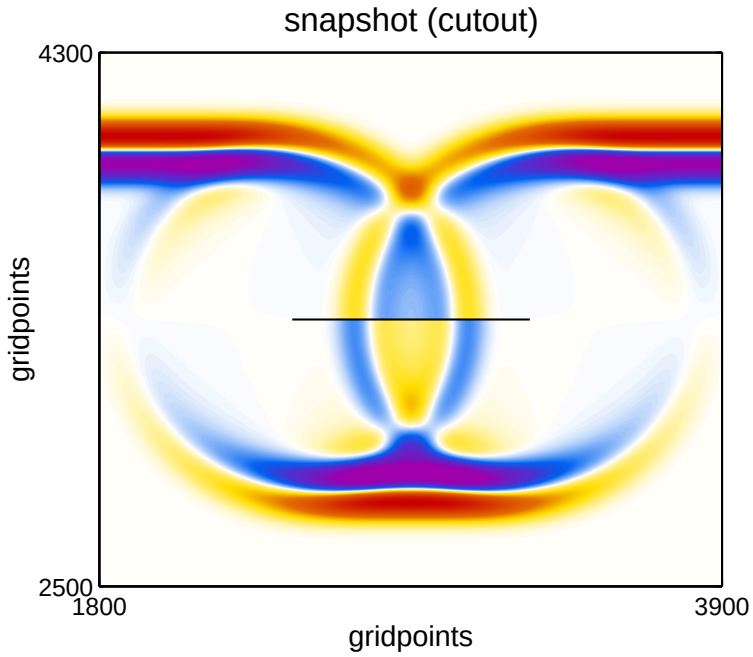

Figure 4: The diffraction of the at the bottom generated plane wave can be observed at the illuminated and the shaded side of the rectilinear crack.

with:

$\tilde{x}$	normalized position in [-1;1]
x	geophone position in [-a;a]
a	half crack length
$\tilde{f}$	normalized frequency
f	frequency of the seismogram spectrum
v_s	S-wave velocity

Discussion

The comparison of analytical and numerical derived power spectra shows an astonishing conformity for a vast range of frequencies, especially for the dominant frequency at $\tilde{f}_{dom} \approx 2.72$ (see Fig 5). It was expected that higher frequencies are not as well resolved as lower frequencies in the numerical solution and a slight difference to the analytical solution is seen (see Fig 6).

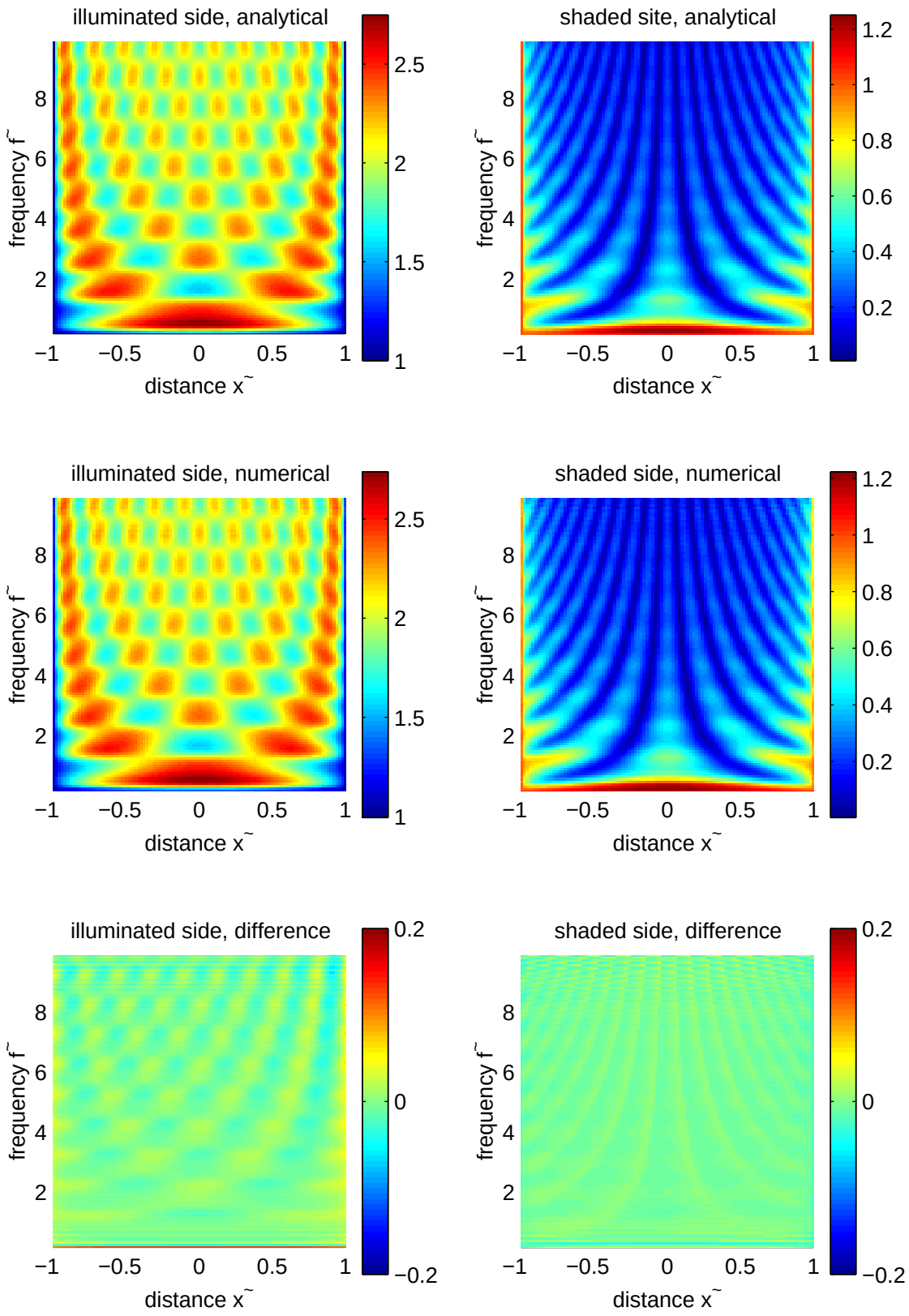

Figure 5: Power spectra at the illuminated and the shadow side of the crack ($\tilde{f}_{dom} \approx 2.72$; for details see text). Please note the low difference between numerical calculation and analytical prediction.

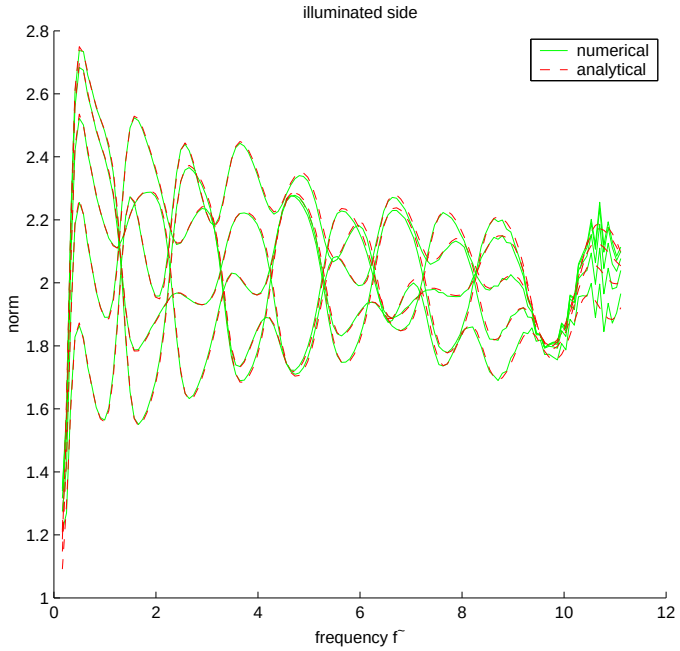

Figure 6: Five typical power spectra of different seismograms recorded at the illuminated side of the crack ($\tilde{f}_{dom} \approx 2.72$) . A comparison with analytical predictions indicate the high accuracy of the rotated staggered grid.

EFFECTIVE VELOCITIES IN 3D FRACTURED MEDIA

Theories of effective moduli

To describe wave propagation in fractured media we consider three different theories for dry penny shaped cracks in 3D-media, namely, the "Kuster-Tuksöz formulation", the "Self-Consistent approximation" and the "Differential Effective Medium (DEM) theory". They can be used to predict effective wave velocities in the long wavelength limit in dependency on porosity ϕ. A detailed review of these rock physical relationships can be found in Mavko et al. (1998). Our goal is to test which theory can be applied for a high crack density. Therefore, in order to compare our numerical results with these three theories we give here their respective effective bulk modulus $< K >$ and effective shear modulus $< \mu >$.

For the case of penny-shaped dry cracks with aspect-ratio α one can obtain the following formulae where K and μ are the bulk modulus and the shear modulus, respectively, of the homogeneous embedding. For the Kuster-Toksöz formulation one obtains:

$$(< K > -K)\frac{K + \frac{4}{3}\mu}{< K > +\frac{4}{3}\mu} = -\phi K P, \tag{22}$$

$$(< \mu > -\mu)\frac{\mu + \zeta}{< \mu > +\zeta} = -\phi \mu Q. \tag{23}$$

The self-consistent approximation reads:

$$< K > = K\ (1 - \phi P), \tag{24}$$

$$< \mu > = \mu\ (1 - \phi Q). \tag{25}$$

The differential effective medium (DEM) can be expressed by two coupled linear differential equations with initial conditions $< K(0) >= K$ and $< \mu(0) >= \mu$ which can be solved numerically:

$$(1 - \phi)\frac{d}{d\phi}[< K(\phi) >] = - < K(\phi) > P(\phi), \tag{26}$$

$$(1 - \phi)\frac{d}{d\phi}[< \mu(\phi) >] = - < \mu(\phi) > Q(\phi), \tag{27}$$

with:

$$P = \frac{K}{\pi\alpha\beta}, \tag{28}$$

$$Q = \frac{1}{5} * \left[1 + \frac{8\mu}{\pi\alpha(\mu + 2\beta)} + \frac{4\mu}{3\pi\alpha\beta}\right], \tag{29}$$

and

$$\beta = \mu\frac{3K + \mu}{3K + 4\mu}, \tag{30}$$

$$\zeta = \frac{\mu}{6}\frac{9K + 8\mu}{K + 2\mu}. \tag{31}$$

Numerical setup

As described above, the rotated staggered FD scheme is a powerful tool for testing theories about fractured media. In order to test the three theories mentioned above we design some numerical elastic models which include a region with a well known number of cracks and porosity. The cracked region was filled at random with randomly oriented penny-shaped cracks. In Figure 7(a) we can see a typical model. This model contains 804 $\times$ 400 $\times$ 400 grid points with an interval of 0.0002m. In the homogeneous region we set $v_p = 5100\ m/s$, $v_s = 2944\ m/s$ and $\rho_g = 2540\ kg/m^3$. For the dry penny-shaped cracks ($\alpha \approx 1/30$) we set $v_p = 0\ m/s$, $v_s = 0\ m/s$ and $\rho_g = 0.0001\ kg/m^3$ which approximate vacuum. It is important to note that we perform our modeling experiments with periodic boundary conditions in the two horizontal directions. For this reason our elastic models are generated also with this periodicity. Hence, it is possible for a single crack to start at the right side of the model and to end at its left side. To obtain effective velocities in different models we apply a body force plane source at the top of the model. The plane wave generated in this way propagates through the fractured medium (see Figure 7(b)). With two horizontal planes of geophones at the top and at the bottom, it is possible to measure the time-delay of the mean peak amplitude of the plane wave caused by the inhomogeneous

region. With the time-delay one can estimate the effective velocity. The source wavelet in my experiments is always the first derivative of a Gaussian with a dominant frequency of $8 * 10^5\ 1/s$ and with a time increment of $\Delta t = 2.1 * 10^{-9} s$. From the modeling point of view it is important to note that all computations are performed with second order spatial FD operators and with a second order time update. Due to the size of the models we have to use large-scale computers (e.g. CRAY T3E) with a MPI implementation of our modeling software.

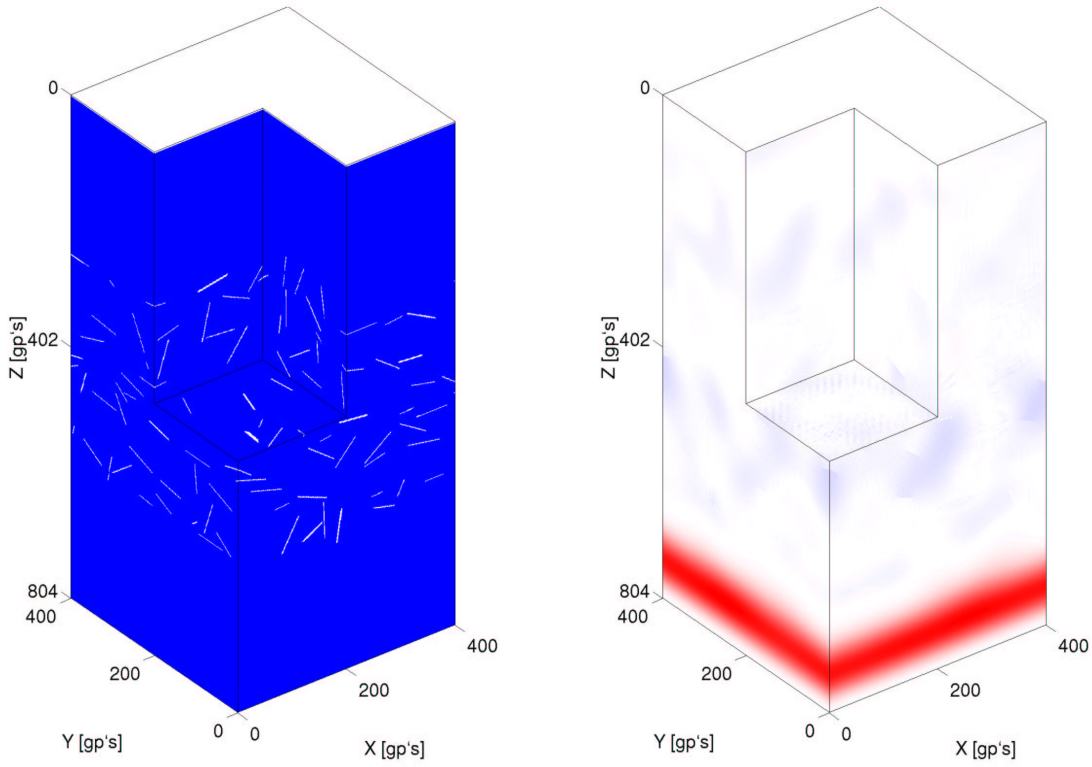

(a) Model; 1 gridpoint $\equiv$ 0.0002m

(b) Wavefield at T = 2000 Δt

Figure 7: The left hand side shows a typical 3D fractured model with non-intersecting penny-shaped cracks used for the numerical experiments. We introduce a cracked region (400 $\times$ 400 $\times$ 400 gridpoints) in a homogeneous material. At the top we place a small strip of vacuum. This is advantageous for applying a body force plane source with the rotated staggered grid. The right side is a displacement-snapshot of a plane wave propagating through the model.

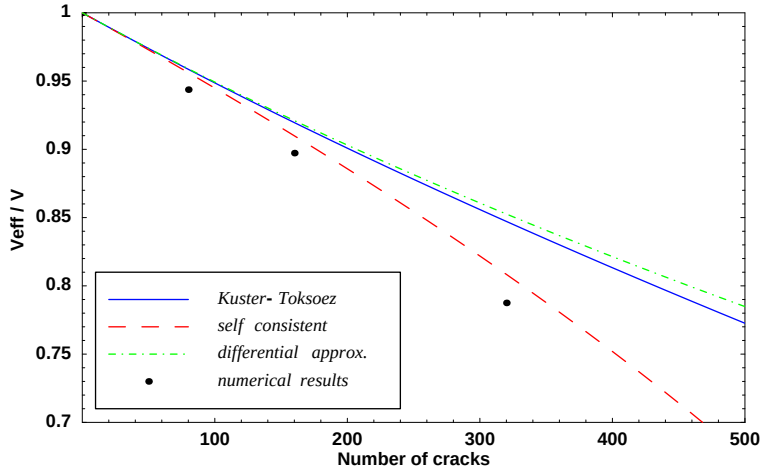

Figure 8: Normalized effective velocity of compressional (*P*-) waves versus number of penny-shaped cracks. Dots: Numerical results of this study. The dashed line is predicted by the self consistent approximation. The dashed-dotted line is the prediction by differential effective medium (DEM) theory and the solid line is due to the Kuster-Toksöz approach.

Numerical results

Our numerical results for penny-shaped dry cracks can be seen in Figure 8. We show the relative decrease of the effective velocity in dependence of the number of cracks. The results and the self-consistent approximation (see Mavko et al. (1998)) are in a good agreement.

CONCLUSIONS

We present a numerical tool, the rotated staggered FD grid, to calculate effective velocities in fractured media. Finite-difference modeling of the elastodynamic wave equation is very fast and accurate. In contrast to a standard staggered grid, high-contrast inclusions do not cause instabilities for the rotated staggered grid (RSG). The RSG can be applied for velocity-stress and for displacement-stress schemes. A comparison of an analytical solution with our numerical tool for a single crack demonstrates the accuracy of our FD scheme. Thus, our numerical modeling of elastic properties of dry rock skeletons can be considered as an efficient and well controlled computer experiment. For 3D fractured models first results are discussed.

PUBLICATIONS

Detailed results regarding the rotated staggered grid and tests of rock physical relationships were published by Saenger et al. (2000), Saenger et al. (2001) and Saenger and Shapiro (2001).

ACKNOWLEDGMENTS

This work was kindly supported by the sponsors of the *Wave Inversion Technology (WIT) Consortium*, Berlin, Germany.

REFERENCES

Bohlen, T. (1998). *Viskoelastische FD-Modellierung seismischer Wellen zur Interpretation gemessener Seismogamme*. PhD thesis, University of Kiel.

Dablain, M. A. (1986). The application of high-order differencing to the scalar wave equation. *Geophysics*, 51:54–66.

Karrenbach, M. (1995). *Elastic tensor wavefields*. PhD thesis, Stanford University.

Kelly, K. R., Ward, R. W., Treitel, S., and Alford, R. M. (1976). Synthetic seismograms: A finite-difference approach. *Geophysics*, 41:2–27.

Mavko, G., Mukerji, T., and Dvorkin, J. (1998). *The Rock Physics Handbook*. Cambridge University Press, Cambridge.

Moczo, P., Kristek, J., and Halada, L. (2000). 3d 4th-order staggered-grid finite-difference schemes: Stability and grid dispersion. *Bulletin of the Seismological Society of America*, page in press.

Robertsson, J. A., Blanch, J. O., and Symes, W. W. (1994). Viscoelastic finite difference modeling. *Geophysics*, 59:1444–1456.

Saenger, E. H., Gold, N., and Shapiro, S. A. (2000). Modeling the propagation of elastic waves using a modified finite-difference grid. *Wave Motion*, 31(1):77–92.

Saenger, E. H., Priller, H., Grosse, C., Hubral, P., Müller, T. M., Sick, C., and Shapiro, S. A. (2001). Wave propagation in heterogeneous media. In *High Performance Computing in Science and Engineering '01*, page in press. Springer.

Saenger, E. H. and Shapiro, S. A. (2001). Effective velocities in fractured media: A numerical study using the rotated staggered finite-difference grid. *Geophysical Prospecting*, page in press.

Sánchez-Sesma, F. J. and Iturrarán-Viveros, U. (2001). Scattering and diffraction of sh waves by a finite crack: an analytical solution. *Geophys. J. Int.*, 145:749–758.

Virieux, J. (1986). Velocity-stress finite-difference method. *Geophysics*, 51:889–901.